

Data-Driven Probabilistic Air-Sea Flux Parameterization

Jiarong Wu¹, Pavel Perezhogin¹, David John Gagne², Brandon G. Reichl³,
Aneesh C. Subramanian⁴, Elizabeth J. Thompson⁵, and Laure Zanna¹

¹Courant Institute of Mathematical Sciences, New York University, New York, NY, USA

²National Center for Atmospheric Research, Boulder, CO, USA

³NOAA – Geophysical Fluids Dynamics Laboratory, Princeton, NJ, USA

⁴Department of Atmospheric and Oceanic Sciences, University of Colorado Boulder, Boulder, CO, USA

⁵NOAA Physical Sciences Lab, Boulder, CO, USA

Key Points:

- We propose a probabilistic air-sea turbulent momentum and heat flux algorithm based on neural networks trained on in-situ observations.
- Our algorithm quantifies the uncertainty (variability) around the mean, with a mean prediction similar to existing bulk algorithms.
- Marked seasonal responses are obtained in deterministic and stochastic tests performed on forced single-column upper-ocean model GOTM.

arXiv:2503.03990v2 [physics.ao-ph] 5 Nov 2025

Corresponding author: Jiarong Wu, jiarong.wu@nyu.edu

Abstract

Accurately quantifying air-sea fluxes is important for understanding air-sea interactions and improving coupled weather and climate models. This study introduces a probabilistic framework to represent the highly variable nature of air-sea fluxes, which is missing in deterministic bulk algorithms. Assuming Gaussian distributions conditioned on the input variables, we use artificial neural networks and eddy-covariance measurement data to estimate the mean and variance by minimizing negative log-likelihood loss. The trained neural networks provide alternative mean flux estimates to existing bulk algorithms, and quantify the uncertainty around the mean estimates. A stochastic parameterization of air-sea turbulent fluxes can be constructed by sampling from the predicted distributions. Tests in a single-column forced upper-ocean model suggest that changes in flux algorithms influence sea surface temperature and mixed layer depth seasonally. The ensemble spread in stochastic runs is most pronounced during spring restratification.

1 Introduction

The atmosphere and ocean exchange mass, momentum, and heat across the air-sea interface. These fluxes influence ocean and atmosphere processes across a vast range of scales. However, quantifying air-sea fluxes is challenging, and significant uncertainties remain (Cronin et al., 2019).

In this work, we focus on momentum flux (denoted as τ_x and τ_y), and on turbulent heat flux (THF), which is a non-radiative heat flux consisting of sensible heat flux (Q_S) due to air-sea temperature difference and latent heat flux (Q_L) due to air-sea humidity difference. Direct in-situ observations of these turbulent fluxes from atmosphere to ocean rely on measuring the covariances of turbulent fluctuations:

$$\tau_x = -\rho_a \overline{u'w'}, \tau_y = -\rho_a \overline{v'w'}, Q_S = -\rho_a c_p \overline{w'T'}, Q_L = -\rho_a L_e \overline{w'q'}. \quad (1)$$

Here u' , v' , w' , T' , and q' are fluctuations of three velocity components, potential temperature, and specific humidity; ρ_a is the air density; c_p is the specific heat capacity at constant pressure, and L_e is the latent heat of evaporation. The measurements are taken in the atmospheric surface layer, where these fluxes are assumed to be constant (Fairall et al., 1996).

The challenges of quantifying these fluxes lie in both observational and modeling aspects. Due to the requirements of sophisticated instruments and careful quality control, such direct measurements are usually carried out on designated research cruises (Bradley & Fairall, 2006). Less equipped measuring platforms and remote sensing measure atmospheric and oceanic surface variables (wind speed, temperature, humidity, etc.) and rely on a bulk flux algorithm to compute the fluxes from the mean observed variables. The same algorithm is used in coupled weather and climate models to compute fluxes based on prognostic state variables of the oceanic and atmospheric surfaces.

The widely used flux algorithms are termed bulk algorithms because they use bulk quantities from the surface layer to model surface fluxes. The momentum and turbulent heat fluxes are formulated as proportional to the magnitude of wind speed $|U_a|$ and air-sea difference in velocity, temperature, and humidity

$$\tau_x = \rho_a C_D S (U_a - U_o), Q_S = \rho_a c_p C_H S (T_a - T_o), Q_L = \rho_a L_e C_E S (q_a - q_s), \quad (2)$$

where C_D , C_H , and C_E are the transfer coefficients for momentum, sensible, and latent heat, respectively. S is the scalar wind speed relative to the ocean surface (subject to gustiness correction). Here, τ_x is aligned with the surface wind and the cross-wind component τ_y is assumed to be zero. The transfer coefficients are calculated based on the Monin-Obukhov similarity theory, where certain parameters (stability function and roughness length) are empirically determined from observations; see a complete description in, e.g., Fairall et al. (2003) for COARE algorithm.

Currently, there are different bulk algorithms, fitted to different sets of observations (Brunke et al., 2003; Biri et al., 2023). Varying levels of simplifications and empirical corrections (e.g., cool-skin warm-layer or gustiness corrections) also exist. This source of uncertainty affects flux estimation in general circulation models (GCMs) and flux products. Sensitivity studies have shown that changes in bulk algorithms can considerably affect atmospheric dynamics (Hsu et al., 2022; Harrop et al., 2018; Polichtchouk & Shepherd, 2016) and oceanic state (Bonino et al., 2022). Flux products also suffer from uncertainty in bulk algorithms, in addition to uncertainty in bulk inputs (Yu, 2019). Due to the prohibitive computational cost of high-fidelity numerical simulations, eddy-covariance (EC) measurements remain our best “ground-truth” for calibrating bulk algorithms, despite their sparsity and intrinsic measurement uncertainty (Gleckler & Weare, 1997). In this study, we use a quality-controlled research vessel cruise dataset provided by NOAA Physical Sciences Lab (PSL) to develop an alternative data-driven flux algorithm.

Another potential drawback of deterministic bulk algorithms is the lack of variability. Bulk algorithms are simplified representations of the underlying dynamical processes and, at best, represent a statistically averaged value of fluxes given the observables. There is a significant spread of EC flux data around the prediction of bulk algorithms. Such deviations from the mean flux values may be crucial for modeling processes on small and fast scales (Nuijens et al., 2024); they can also have a rectifying effect for large-scale dynamics in nonlinear GCMs. More complex formulas such as sea-state-dependent parameterization (Edson et al., 2013; Bouin et al., 2024) have been proposed that incorporate additional sources of variability, but have not yet been fully validated and widely adopted.

We aim to quantify the uncertainty (variability) around deterministic flux algorithms in EC data while taking an agnostic perspective on its sources. This is achieved by applying a framework based on conditional parametric probability distributions (Nix & Weigend, 1994; Barnes et al., 2021; Guillaumin & Zanna, 2021; Schreck et al., 2024). In particular, we use artificial neural networks (ANNs) to approximate the distribution parameters. Recent advances in machine learning have led to its applications in surface flux parameterization (Bourras et al., 2007; Leufen & Schädler, 2019; McCandless et al., 2022; Cummins et al., 2024; Zhou et al., 2024), although mainly for point estimates. In most of the paper, we use the terms “uncertainty” and “variability” interchangeably to refer to the spread in observed data, but its attribution will be discussed in the end.

An estimate of uncertainty around deterministic bulk algorithms will benefit uncertainty quantification in downstream applications such as flux products and stochastic air-sea flux parameterization. Stochastic parameterizations have been shown to improve the representation of low-frequency variability and to reduce bias in the mean state (Williams, 2012; Andrejczuk et al., 2016; Juricke et al., 2017; Berner et al., 2017). In particular, air-sea fluxes are expected to play a significant role in the upper ocean. However, the sensitivity of the upper ocean states to uncertainty in the flux algorithm is not yet well quantified. We implement our probabilistic flux algorithm in the single-column General Ocean Turbulence Model (GOTM, Umlauf and Burchard (2005)) to study the effects on the upper ocean states.

2 Data and model

2.1 Direct in-situ covariance measurements

The air-sea flux observation dataset we use is collected by decades of research cruises conducted by NOAA PSL. There are about 10,000 samples after quality control, and all are ship-borne, hourly-averaged covariance measurements according to Equation 1. The trajectories of the various cruises are shown in Figure 1(a). Among the labeled cruises, Metz is a compilation of multiple earlier cruises in the 1990s; WHOTS, EPIC, DYNAMO are conducted in the tropics and Stratus in the subtropics; Calwater, NEAQS, HiWInGS

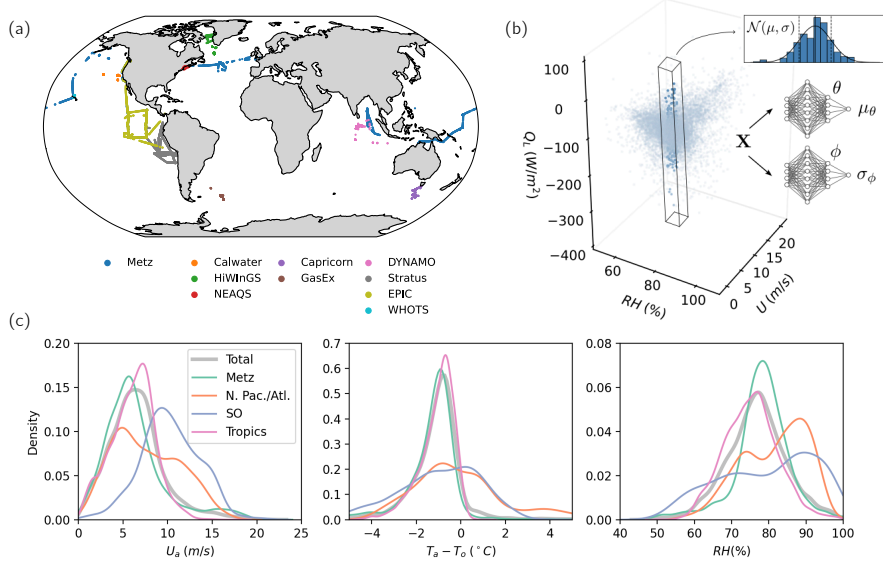


Figure 1. (a) Ship trajectories of the various cruises in the NOAA PSL dataset. (b) An illustration of the ANN-based conditional Gaussian probabilistic model. Note that we are visualizing only two of the input space dimensions, for the purpose of showing the concept of a conditional Gaussian distribution. (c) Distributions of input variables for different subsets of data.

in mid/high latitudes of the northern hemisphere, and Capricorn, GasEX in the southern ocean. Overall, this dataset covers various geographical locations, although a disproportional amount of data is collected in the tropics (more than 50%). We note that analyzing the measurements taken along transects as time series will likely reveal additional embedded information, but in this study we treat them as independent samples of the underlying conditional distribution.

2.2 Probabilistic model

We consider observed bulk variables \mathbf{X} (such as wind speed, humidity, etc.), unobserved variables \mathbf{Z} (for example sea state, vertical wind profile, etc.), and targeted flux outputs $\mathbf{Y} = (\tau_x, \tau_y, Q_S, Q_L)$. Due to the unobserved variables \mathbf{Z} , the relation $\mathbf{Y} = \mathbf{F}_{model}(\mathbf{X})$ is not deterministic even when the physical laws governing the fluxes $\mathbf{Y} = \mathbf{F}_{true}(\mathbf{X}, \mathbf{Z})$ are deterministic. Using the proposed probabilistic model, we account for all uncertainties in the data, and further attributions are discussed in Section 5.

We assume that each flux component y of \mathbf{Y} follows a uni-variate conditional Gaussian distribution with mean $\mu(\mathbf{X})$ and standard deviation (std) $\sigma(\mathbf{X})$:

$$y \sim \mathcal{N}(\mu(\mathbf{X}), \sigma^2(\mathbf{X})). \quad (3)$$

In other words, $\mu(\mathbf{X})$ is our best unbiased estimation of the flux component y given \mathbf{X} , and the errors are distributed according to $\mathcal{N}(0, \sigma^2(\mathbf{X}))$ when conditioned on \mathbf{X} . This idea of conditional Gaussian distribution is demonstrated in Figure 1(b) with the latent heat flux data.

Having chosen the parametric distribution, we aim to learn the parameters $\mu_\theta(\mathbf{X})$ and $\sigma_\phi^2(\mathbf{X})$ with the given data. Here θ and ϕ denote the learnable parameters in the data-driven models for μ and σ^2 . The optimization procedure is based on computing the probability as a function of parameters (i.e., likelihood) of observing a sample value y given

the sample input features \mathbf{x} :

$$p(y|\mathbf{x}, \theta, \phi) = \frac{1}{\sqrt{2\pi\sigma_\phi^2(\mathbf{x})}} \exp \left[-\frac{(y - \mu_\theta(\mathbf{x}))^2}{2\sigma_\phi^2(\mathbf{x})} \right]. \quad (4)$$

The optimal model parameters θ and ϕ minimize this negative log-likelihood loss, computed on the training dataset summed over a total of N_{sample} (Nix & Weigend, 1994):

$$L_{\text{null}}(\theta, \phi) = \sum_{m=1}^{N_{\text{sample}}} \frac{1}{2} \left[\log(\sigma_\phi^2(\mathbf{x}_m)) + \frac{(y_m - \mu_\theta(\mathbf{x}_m))^2}{\sigma_\phi^2(\mathbf{x}_m)} \right] + \text{const.} \quad (5)$$

2.3 ANN architecture and training

The mathematical framework described in Section 2.2 is general and applies to any data-driven model that approximates parametric distributions. In particular, as shown in Figure 1(b), we use two ANNs to represent the mean μ_θ and the variance σ_ϕ^2 for each flux component. In this case, θ and ϕ are the weights and biases of the ANNs. The non-linear activation function of the hidden layers is the Sigmoid function. The positivity of the predicted variance σ_ϕ^2 is ensured with the exponential activation function in the last ANN layer.

The input variables are selected based on a balance between expressibility and the risk of overfitting, as well as practical considerations for the typically available variables in GCMs. After testing different numbers of inputs and their combinations, we have chosen five inputs

$$\mathbf{X} = (U_a, T_a, T_o, RH, p_a) \quad (6)$$

which are wind speed (measured between 16 to 21 m), atmospheric surface temperature (measured between 12 to 19.5 m), sea surface temperature (measured by sea snake at 0.05 m depth), relative humidity (measured between 12 to 19.5 m), and atmospheric pressure at sea surface. Using relative humidity instead of specific humidity gives better behaviors during training, although the two can be converted given atmospheric temperature and pressure. We do not include the heights at which the meteorological variables are measured, although they are used as inputs to existing bulk algorithms. This is mainly because the ship-borne sensors are placed at a height where the vertical gradient of the atmospheric surface variables is vanishing and the height dependence cannot be explicitly learned. This is not a problem for climate-scale GCMs, which have a coarse vertical resolution, but it is a potential caveat when applied to low-lying platforms, such as buoys.

The training of ANNs is described in detail in the supplementary information. Briefly summarized here, we first train the networks on mean-square error loss and then on negative log-likelihood loss (Equation 5). This two-step procedure allows the mean ANN to capture more variability in the data. The small data limit and the distribution shift shown in Figure 1(c) are challenging for data-driven models, which we overcome through input feature selection, model design, training strategies (such as early stopping), and cross-validation.

Having learned the parametric distribution of the fluxes for the given inputs, predictions can be made in two ways: using the mean μ_θ for deterministic predictions or sampling from the distribution $\mathcal{N}(\mu_\theta, \sigma_\phi^2)$ for stochastic predictions. In Section 3.1, we evaluate the statistical scores of the deterministic predictions. In Section 3.2, we analyze the predicted dependence of μ_θ and σ_ϕ^2 on inputs. In Section 4, numerical experiments using both deterministic and stochastic heat fluxes are discussed. For simplicity, we denote the mean predictions as $(\mu_{\tau_x}, \mu_{\tau_y}, \mu_{Q_S}, \mu_{Q_L})$ and the variance predictions as $(\sigma_{\tau_x}^2, \sigma_{\tau_y}^2, \sigma_{Q_S}^2, \sigma_{Q_L}^2)$, omitting subscript θ and ϕ .

3 Evaluation of the ANN-based probabilistic air-sea flux model

3.1 Statistical scores of the deterministic predictions

We evaluate the statistical scores of the flux predictions in terms of the root-mean-square-error RMSE, the coefficient of determination R^2 , and bias of the estimate (compared to observations):

$$\text{RMSE}(\hat{y}, y) = (\mathbb{E}[(\hat{y} - y)^2])^{1/2}, \quad (7)$$

$$R^2(\hat{y}, y) = 1 - \mathbb{E}[(\hat{y} - y)^2] / \text{Var}[y], \quad (8)$$

$$\text{Bias}(\hat{y}, y) = \mathbb{E}[\hat{y} - y] \quad (9)$$

Here \hat{y} is the algorithm prediction and y is the truth, in our case the EC measurement $(\tau_{x,c}, \tau_{y,c}, Q_{S,c}, Q_{L,c})$. We evaluate these metrics for the ANN-based deterministic prediction $(\mu_{\tau_x}, \mu_{\tau_y}, \mu_{Q_S}, \mu_{Q_L})$ compared to a baseline bulk algorithm $(\tau_{x,b}, 0, Q_{S,b}, Q_{L,b})$. In particular, we choose COARE 3.6 (Fairall et al., 2003), which is the most up-to-date version of COARE. It is worth mentioning that COARE was fitted to the same shipborne EC data we used, with additional cruises and buoy measurements.

Figure 2(a) shows the flux predictions plotted against the EC measurements. ANN-based deterministic predictions have similar but slightly higher R^2 than COARE for all three fluxes, see legends in Figure 2(a), with only a subset of the input variables. For the cross-wind momentum flux τ_y (not shown here), ANN-based deterministic prediction has little predictive skills, as there is no input variable to indicate the sign of cross-wind stress. Without additional input features (such as surface wave information), it is reasonable to accept zero prediction as is in bulk algorithms. However, we can quantify the variability around the zero prediction with the current framework.

The statistical scores of both ANN and COARE vary considerably between different turbulent fluxes. The sensible heat flux Q_S is the hardest to predict for both based on its lowest R^2 values, while the latent heat flux Q_L gives the largest magnitude of error in terms of RMSE. Another observation is that scores of both ANN and COARE also vary considerably between geographical locations. Figure 2(b) shows R^2 and bias of three fluxes evaluated on different subsets of cruises grouped roughly by geographical locations (same as in Figure 1). This is because each geographical subset has substantially different distributions of the input variable, as shown in Figure 1(c). In particular, R^2 for sensible heat flux Q_S is very low in the Tropics, only around 0.15. This is partly because the variance of the sensible heat flux is small in the Tropics. Overall, the fluctuation of predictive scores over different regions is shared between ANN and COARE.

The most salient improvement of ANN compared to baseline bulk algorithm is for latent heat flux, which is generally the least constrained of all turbulent fluxes. In certain regions, ANN improves R^2 up to about 0.2 increase in R^2 . Overall, we notice that the estimate of latent heat given by bulk algorithm seems biased (towards predicting more evaporation from the ocean), and ANN fix the bias to some extent, as shown in Figure 2(b). This bias correction in latent heat flux was also found in a recent paper using data-driven method (Zhou et al., 2024) and may have important implications for global simulations. Supplementary table S1 lists RMSE and R^2 evaluated on the full dataset and on different geographical subsets. The reason underlying the statistical improvement is likely that the flexible structure of ANN provides more expressibility, and therefore fits the data better where certain assumptions of traditional bulk algorithms break down, e.g., the logarithmic profile for humidity and the expression for scalar roughness lengths. This idea is further discussed in the supplementary information and ANN predictions in terms of transfer coefficients C_D , C_H , and C_E are also shown (Figure S1).

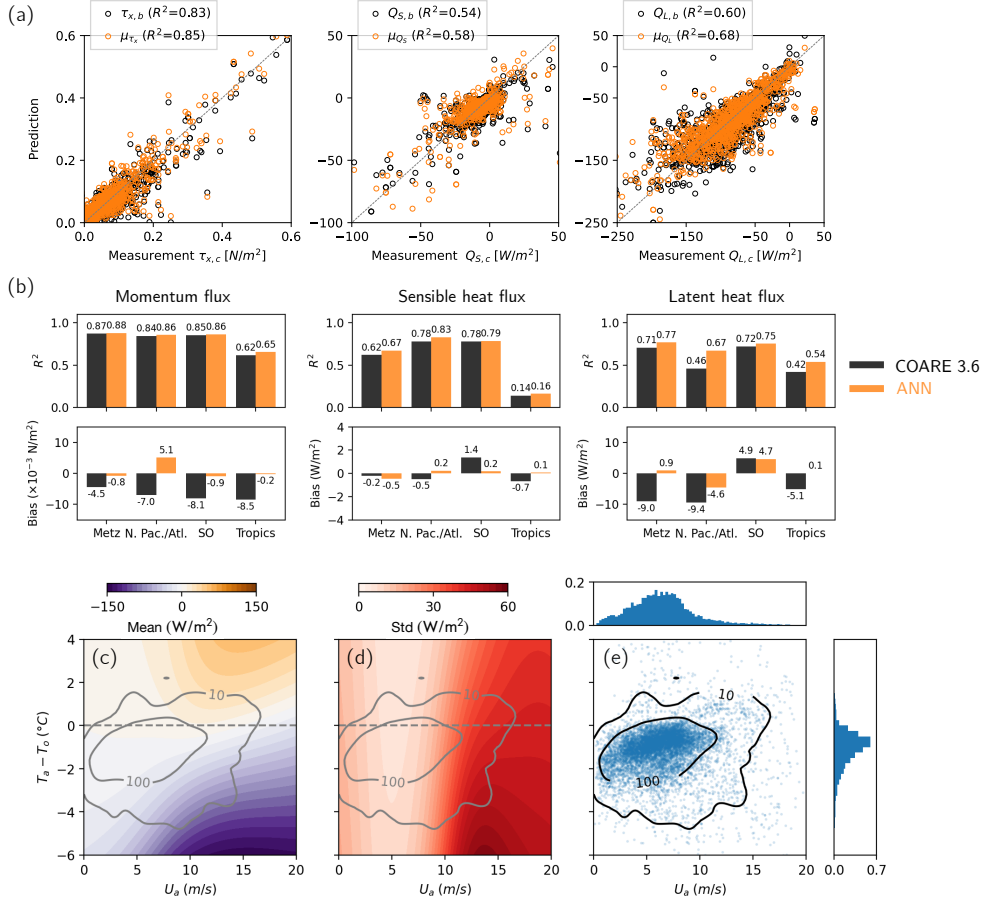


Figure 2. (a) ANN-based deterministic predictions (orange dots) and bulk algorithm predictions (black dots) plotted against measured fluxes. We are only visualizing 10% of total samples. (b) R^2 and bias of ANN (orange) and bulk algorithm (black), evaluated on different geographical subsets. (c) ANN prediction of the mean of Q_S on a uniform input grid. The dashed gray lines mark zero temperature difference $T_a = T_o$. (d) ANN prediction of the std of Q_S for the same grid. (e) Scatter plot of all data points and their marginal distribution. Gaussian kernel density estimation provides the gray contour lines that indicate the available samples per unit ΔU and $\Delta(T_a - T_o)$. The same contour lines are overlaid on (c) and (d).

3.2 Structure of the mean and variance predicted by ANNs

In addition to the statistical scores, we further evaluate the ANN predictions on a reduced-dimension uniform grid to probe and interpret the ANN flux model. This is especially important for the std σ as a way to understand how the predicted std depends on input variables. Figure 2(c) and (d) illustrate this using sensible heat flux as an example. Among the five inputs, we fix sea surface temperature $T_o = 10^\circ\text{C}$, relative humidity $RH = 80\%$, and sea level pressure $p_a = 1010\text{ hPa}$, while varying wind speed U_a and temperature difference $T_a - T_o$. The plot represents a 2D slice of the 5D input space with typical values for the other variables.

Figure 2(c) shows the prediction of Q_S mean by ANN, which is smooth and asymmetric around $T_a - T_o = 0$. Unlike bulk algorithms that assume $Q_{S,b} \propto S(T_a - T_o)$, the structure of ANN is more flexible, allowing non-zero flux values even when $T_a = T_o$.

A similar figure for COARE is shown in [supplementary Figure S1 \(check all figure numbers\)](#). We did not impose any constraints on the sign of Q_S , contrary to Zhou et al. (2024), which used a penalty in the loss function to ensure matching signs of $T_a - T_o$ and Q_S . In our experience, such a penalty is not necessary for a good statistical fit. Furthermore, there is insufficient evidence for a strictly down-gradient assumption, since locally counter-gradient fluxes are possible (Blay-Carreras et al., 2014; Deardorff, 1972) and systematic bias in measurements may exist.

Figure 2(d) shows the prediction of std of Q_S for the same grid. Uncertainty increases with wind speed, as expected, since residuals should scale with flux magnitude to some extent. A small but finite uncertainty persists at very low wind speeds, likely due to measurement challenges associated with small fluxes. For a given wind speed, the uncertainty is consistently higher for $T_a < T_o$, corresponding to unstable boundary layer conditions. As shown in Figure 2(e), data are sparse for wind speeds above 15 m/s and large temperature differences. While the ANN seems to extrapolate reasonably well, it is worth exploring methods to further constrain it where training samples are not available. We note that the same issue applies to existing bulk algorithms as well.

4 Tests: surface flux forced upper ocean mixing

As a preliminary test for the proposed probabilistic air-sea flux model, we choose to implement it in the single column model GOTM (Umlauf & Burchard, 2005), which provides a controlled environment with no complex interplay with other nonlinear processes in GCMs. The governing equations are a set of 1D diffusion-type equations

$$\partial_t u = -\partial_z \overline{w'u'} + fv, \quad \partial_t v = -\partial_z \overline{w'v'} - fu, \quad \partial_t T = -\partial_z \overline{w'T'}, \quad \partial_t S = -\partial_z \overline{w'S'}, \quad (10)$$

where the prognostic variables are the horizontal velocity components u and v (subject to Coriolis force), temperature T , and salinity S . The turbulent fluxes $\overline{w'u'}$, $\overline{w'v'}$, $\overline{w'T'}$, $\overline{w'S'}$ are not resolved but are instead parameterized by vertical mixing schemes. In particular, we test our air-sea flux algorithms in combination with two ocean surface boundary layer (OSBL) mixing parameterizations: the K-profile-parameterization (KPP) scheme (Large et al., 1994) and a more sophisticated second-order closure $k-\epsilon$ scheme (Umlauf & Burchard, 2005), both used in GCMs but typically under different resolutions.

Air-sea momentum and heat fluxes serve as boundary conditions to Equation 10. Additionally, surface fluxes can impact the mixing parameterization. In the KPP scheme, a change in heat flux (therefore buoyancy flux), affects the OSBL depth through the Richardson number criterion, and the sign of buoyancy flux determines the shape function (Large et al., 1994). In the $k-\epsilon$ scheme, the production terms in the turbulence kinetic energy (TKE) equation are affected by surface fluxes.

4.1 Heat flux time series at OWS Papa

We use Ocean Weather Station (OWS) Papa (50°N, 145°W) as our test site. This long-term North Pacific station provides hourly meteorological and oceanic measurements, including temperature and salinity profiles. Its weak horizontal advection makes it a common benchmark for testing vertical mixing parameterization in single-column models (Umlauf & Burchard, 2005; Li et al., 2021). We discuss the flux predictions given the observed input variables at OWS Papa before showing results from the forced experiments.

Figure 3(a) shows an example of ANN-predicted (deterministic) THF time series $Q = \mu_{Q_S} + \mu_{Q_L}$, compared to bulk algorithms, zoomed in to July and October 2015. We plot two bulk algorithms - COARE 3.6 and NCAR (Large & Yeager, 2009) - to show that the ANN deviations exceed those between different bulk algorithms. This confirms that ANN is structurally different from any bulk algorithm. As with the THF itself, the difference between the ANN and bulk predictions is seasonal, as the input distributions

vary throughout the year. This seasonality can be seen in Figure 3(c), which shows the monthly averaged flux discrepancy between ANN and COARE 3.6. The months of July and October see the most negative (more heat flux out of the ocean) and positive (less heat out) differences. Notice that within a period of high THF around Oct 10, ANN predicts the least extreme negative values while NCAR predicts the most extreme negative value, reflecting all three algorithms' divergence at high wind speed, where few measurements exist to constrain them.

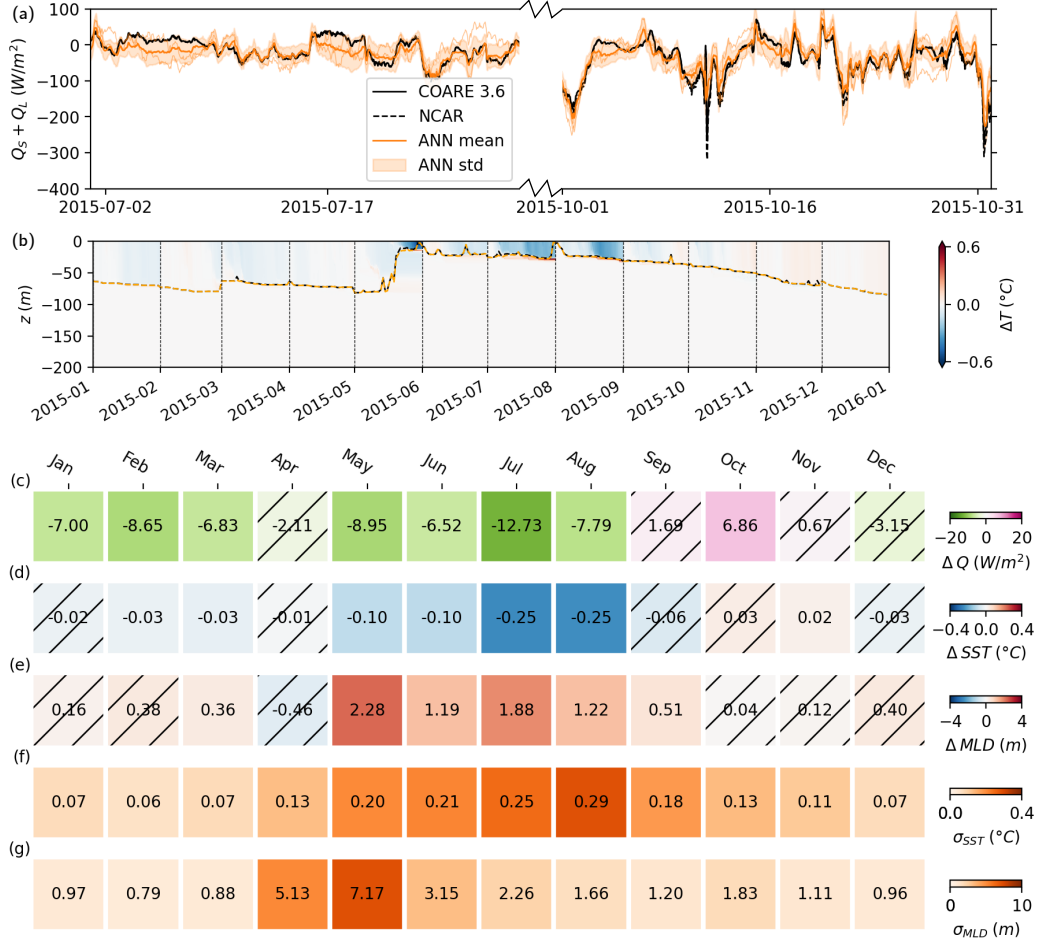


Figure 3. (a) Example THF time series for July and October 2015, computed using observed input variables at OWS Papa. Black solid line: COARE 3.6; black dashed: NCAR; orange line: ANN. Orange shade shows one standard deviation for THF predicted by ANN, which is used to generate noise-perturbed heat fluxes (examples shown by thin orange lines). (b) Difference of temperature profiles in the deterministic single-column run $\Delta T(z, t) = T_{ANN}(z, t) - T_{bulk}(z, t)$. Black and orange dashed lines show the diagnosed MLD for bulk and ANN, respectively. (c) Monthly-averaged THF discrepancies between ANN and COARE. (d) SST and (e) MLD responses in the deterministic runs between (ANN minus COARE). Trends with inconsistent signs over the years are masked with hatching. (f) Monthly-averaged SST and (g) monthly-averaged MLD spread in 20 ensemble runs.

Figure 3(a) also shows the ANN-predicted $\pm 1\sigma_Q$ for THF in orange shading. We assume no covariance between the sensible and latent heat flux residuals; therefore, the

uncertainty of their sum simply follows $\sigma_Q^2 = \sigma_{Q_S}^2 + \sigma_{Q_L}^2$. Importantly, the predicted σ_Q is state dependent, so the uncertainty envelope changes over time. Given the ANN-predicted time series of mean and std of THF, we can create an ensemble of stochastically perturbed fluxes. Two examples of such perturbed fluxes are shown with thin orange lines. The stochastic perturbation is expected to stem from certain unobserved processes with characteristic correlation time scales. Therefore, instead of white noise, we use temporally correlated noise ϵ generated through a discrete autoregressive model of order one - AR(1). Similar stochastic perturbation has been applied to momentum flux in the context of studying the diurnal cycle of ocean surface layer (Giglio et al., 2017) but not to heat flux on a seasonal to annual time scale, to our knowledge. The correlation time of 60 hours is estimated from the OWS Papa data (see supplementary information for details). It is also interesting to note that the bulk algorithm predicted THF is generally within $\pm\sigma_Q$, and thus can be interpreted as one possible ensemble member.

There are two parts of the probabilistic flux algorithms to test. First, we evaluate the effects of changing the flux algorithm from COARE 3.6 to ANN-predicted mean in deterministic runs. Second, we examine the uncertainty introduced by surface fluxes to the modeled upper-ocean state by performing ensemble runs using stochastically perturbed fluxes. Details of the numerical experiments are provided in the supplementary information. There is still a known net heat flux imbalance due to the omission of horizontal advection, which we mitigate by restarting the simulation with the observed profiles every month. For this and other reasons discussed in the supplementary information, our analysis emphasizes intercomparison between simulations rather than direct validation against observations, in particular two characteristic quantities: sea surface temperature (SST) and mixed layer depth (MLD).

4.2 Response in deterministic runs

At OWS Papa, the mixed layer is deep in the winter because strong winds and surface cooling induce convective mixing, and shallow in the summer because weaker winds and more radiative heating lead to stable stratification. In spring, as the radiative heating gains and the THF decreases in magnitude, there is a fast restratification process, whereas in fall, the erosion of the stratification is more gradual. This annual cycle is relatively well captured given the monthly restart, as shown in Figure S3.

Figure 3(b) shows the difference in temperature profiles between ANN and COARE flux forced runs, as well as the MLD, for 2015. The composite statistics for four years of monthly-averaged change in SST and MLD are summarized in Figure 3(d) and (e). There is a perceivable response in temperature (fairly uniform across the mixed layer) as a result of a change in surface heat flux. ANN generally predicts more surface heat loss, which deepens the mixed layer and cools the sea surface. When the mixed layer is the shallowest in the summer months, there is the largest change in SST, consistent with a heat budget idea. We note that these effects are consistent across $k-\epsilon$ and KPP (see Figure S6), suggesting an insensitivity to OSBL parameterization.

In summary, switching from COARE 3.6 to ANN can result in differences of up to 2 meters in monthly-averaged MLD and 0.25 degrees in monthly-averaged SST. For context, switching the vertical mixing parameterization from $k-\epsilon$ to KPP can generate a much larger response in monthly averaged MLD, up to 18 meters (see Figure S4). Since perturbing the surface heat flux alone does not appear to generate a big response in MLD, this suggests that it is possible to calibrate surface heat flux and mixing separately, despite their interwoven effects on the upper ocean state. The response to surface heat flux is mainly in the spring and summer (at least at OWS Papa), while the response to mixing extends into the winter months. Future work will test perturbation to momentum flux, which might be dynamically more important.

4.3 Spread in stochastic ensemble runs

The ensemble of forced simulations provides an estimate of the variability in SST and MLD induced by the variability of THF. From the 20 ensemble member runs, we do not observe systematic drift induced by the stochastic forcing; the ensemble mean of the stochastic runs closely tracks the deterministic run (see Figure S5). This is expected since we are performing forced experiments and there is no feedback of state variables (such as SST) to surface forcing.

However, there is a certain level of ensemble spread, which is summarized in Figure 3(f) and (g). Here we focus on the spread in monthly averaged quantities, while the instantaneous spread can be larger (see Figure S5). The largest spread in MLD occurs during the months of April and May, since stochasticity can significantly affect the onset of restratification. This may have important implications for biogeochemical processes, suggesting that comparisons between modeled and observed upper ocean profiles, especially during restratification, may be sensitive to surface THF uncertainty. The largest spread in SST is seen around August, again because the mixed layer is shallow and SST is sensitive to surface heat fluxes. As in deterministic runs, the effects seen in stochastic runs are not particularly sensitive to different OSBL parameterizations.

5 Conclusion and discussion

We propose an ANN-based probabilistic model for turbulent air-sea fluxes. State-of-the-art bulk algorithms represent the statistical mean of eddy-covariance flux observations for a given set of state variables. Our work reinforces this idea by providing an alternative mean estimate using a purely data-driven approach. The ANN-predicted mean is similar to existing bulk algorithms, with marginally higher statistical correlation to data and reduced bias for latent heat flux. Additionally, the ANN-predicted standard deviation around the mean offers a measure of uncertainty (variability). Tests using OWS Papa data and a single-column model show that the difference in THF between the two algorithms' estimates exhibits signs of seasonality, as does the response of upper ocean states, despite relatively small magnitudes. Stochastic ensemble runs indicate that the spread of MLD is largest during spring restratification, while the spread of SST is largest during summer when the mixed layer is shallow.

We comment that the current framework can also be used to estimate the standard deviation around a given mean estimation, e.g., any existing bulk algorithm. In other words, we consider the residual between the observation and the bulk algorithm (or ANN) prediction. It is important to note that the uncertainty we estimate does not distinguish between measurement uncertainty (both instrument and sampling, with sampling uncertainty being the dominant factor) and missing physics (the inability to account for all predictive input variables). Such a partition is difficult and likely depends on the averaging window of the EC flux, which will be examined in future studies. Nonetheless, the ANN-estimated uncertainty highlights regions in the input space where the data is more "scattered". This motivates field campaigns for better sampling of these regimes and examination of measurement uncertainty, as well as the use of high-fidelity numerical simulation to constrain the flux estimate (Clayson et al., 2023).

There are several possible extensions of this work in the future. The ANN model uses a limited set of input variables, which is why the improvement over the existing algorithm may be considered marginal. Further improvement is possible, as several additional variables are measured and available in the dataset (e.g., turbulent kinetic energy). However, we must consider that many of these variables are not yet prognostic variables in GCMs. The height dependence is difficult to learn from the current data set alone, because there is little variance in the measurement height, but incorporating data from other measurement platforms (e.g., buoy) might help. We also need more high-quality

vertical profile measurements of surface wind, temperature, and humidity. The probabilistic model presented assumes a univariate conditional Gaussian distribution for each flux component. This may not fully capture the underlying complexity, especially if the residual is induced by unrepresented physical processes. The model can be extended to include the covariance between flux components, and the Gaussian assumption can be relaxed, given that we have more data to train a more complicated statistical model. Finally, the analysis at OWS Papa provides an initial estimate of the response magnitude but is unlikely to be representative of the global ocean with varying meteo-ocean conditions and coupling dynamics across regions. We plan to extend our analysis to global simulations to assess the broader impact of modified air-sea flux algorithm.

While existing bulk algorithms represent the mean values of turbulent fluxes given limited input variables, our approach takes a step towards examining the variability around the mean values. Stochastic air-sea flux parameterization offers a promising alternative to the deterministic approach. It is crucial to prescribe the appropriate magnitude and correlation scale of noise with varying model resolutions, which needs to be better understood in future studies. In the single-column test, the spread induced by stochastic residuals exceeds that of different deterministic flux algorithms. Therefore, extending the testing to global GCMs could potentially affect the variability and address long-standing biases through interaction with horizontal transport and other nonlinear dynamics.

Open Research Section

The full NOAA PSL cruises are documented and available here <https://downloads.psl.noaa.gov/psd3/cruises/>. For this study we used a compact compilation data set https://github.com/jiarong-wu/mlflux/blob/main/fluxes_all_cruises_compilation.nc. The code for ANN training and evaluation can be found in this repository <https://github.com/jiarong-wu/mlflux>. The GOTM code is available here <https://gotm.net/portfolio/>. In particular, this work used an implementation of GOTM in the PDE solver Basilsik (Popinet, 2020) http://basilisk.fr/src/test/ows_papa.c. For comparison to bulk algorithms, we used the aerobulk-python package <https://github.com/xgcm/aerobulk-python>.

Acknowledgments

This research received support through the National Science Foundation Science and Technology Center, Learning the Earth with Artificial Intelligence and Physics, LEAP (Grant number 2019625). We thank Julia Simpson, Pierre Gentine, and Bia Villas Bôas for helpful discussions and the anonymous reviewers for their useful feedback. Aakash Sane, Qing Li, and Stéphane Popinet provided valuable advice regarding the GOTM implementation. We acknowledge the continued efforts from NOAA PSL lab (including Ludovic Bariteau, Chris Fairall, and many others) in obtaining and publishing the EC datasets. The statements, findings, conclusions, and recommendations are those of the author(s) and do not necessarily reflect the views of the National Oceanic and Atmospheric Administration, or the U.S. Department of Commerce. This research was also supported in part through the NYU IT High Performance Computing resources, services, and staff expertise.

References

- Andrejczuk, M., Cooper, F. C., Juricke, S., Palmer, T. N., Weisheimer, A., & Zanna, L. (2016). Oceanic Stochastic Parameterizations in a Seasonal Forecast System. *Monthly Weather Review*. doi: 10.1175/MWR-D-15-0245.1
- Barnes, E. A., Barnes, R. J., & Gordillo, N. (2021). *Adding Uncertainty to Neural Network Regression Tasks in the Geosciences*. arXiv. doi: 10.48550/arXiv.2109.07250

- Berner, J., Achatz, U., Batté, L., Bengtsson, L., Cámara, A. d. I., Christensen, H. M., . . . Yano, J.-I. (2017). Stochastic Parameterization: Toward a New View of Weather and Climate Models. *Bulletin of the American Meteorological Society*, *98*(3), 565–588. doi: 10.1175/BAMS-D-15-00268.1
- Biri, S., Cornes, R. C., Berry, D. I., Kent, E. C., & Yelland, M. J. (2023). AirSeaFluxCode: Open-source software for calculating turbulent air-sea fluxes from meteorological parameters. *Frontiers in Marine Science*, *9*. doi: 10.3389/fmars.2022.1049168
- Blay-Carreras, E., Pardyjak, E. R., Pino, D., Alexander, D. C., Lohou, F., & Lothon, M. (2014). Countergradient heat flux observations during the evening transition period. *Atmospheric Chemistry and Physics*, *14*(17), 9077–9085. doi: 10.5194/acp-14-9077-2014
- Bonino, G., Iovino, D., Brodeau, L., & Masina, S. (2022). The bulk parameterizations of turbulent air–sea fluxes in NEMO4: the origin of sea surface temperature differences in a global model study. *Geoscientific Model Development*, *15*(17), 6873–6889. doi: 10.5194/gmd-15-6873-2022
- Bouin, M.-N., Lebeaupin Brossier, C., Malardel, S., Voldoire, A., & Sauvage, C. (2024). The wave-age-dependent stress parameterisation (WASP) for momentum and heat turbulent fluxes at sea in SURFEX v8.1. *Geoscientific Model Development*, *17*(1), 117–141. doi: 10.5194/gmd-17-117-2024
- Bourras, D., Reverdin, G., Caniaux, G., & Belamari, S. (2007). A Nonlinear Statistical Model of Turbulent Air–Sea Fluxes. *Monthly Weather Review*, *135*(3), 1077–1089. doi: 10.1175/MWR3335.1
- Bradley, F., & Fairall, C. (2006). *A Guide to Making Climate Quality Meteorological and Flux Measurements at Sea* (Tech. Rep.). NOAA technical memorandum OAR PSD.
- Brunke, M. A., Fairall, C. W., Zeng, X., Eymard, L., & Curry, J. A. (2003). Which Bulk Aerodynamic Algorithms are Least Problematic in Computing Ocean Surface Turbulent Fluxes? *Journal of Climate*.
- Clayson, C. A., DeMott, C., De Szoeke, S., Chang, P., Foltz, G., Krishnamurthy, R., . . . Patterson, M. (2023). *A New Paradigm for Observing and Modeling of Air-Sea Interactions to Advance Earth System Prediction* (Tech. Rep.). U.S. CLIVAR Project Office. doi: <https://doi.org/10.5065/24j7-w583>
- Cronin, M. F., Gentemann, C. L., Edson, J., Ueki, I., Bourassa, M., Brown, S., . . . Zhang, D. (2019). Air-Sea Fluxes With a Focus on Heat and Momentum. *Frontiers in Marine Science*, *6*.
- Cummins, D. P., Guemas, V., Blein, S., Brooks, I. M., Renfrew, I. A., Elvidge, A. D., & Prytherch, J. (2024). Reducing Parametrization Errors for Polar Surface Turbulent Fluxes Using Machine Learning. *Boundary-Layer Meteorology*, *190*(3), 13. doi: 10.1007/s10546-023-00852-8
- Deardorff, J. W. (1972). Numerical Investigation of Neutral and Unstable Planetary Boundary Layers. *Journal of the Atmospheric Sciences*.
- Edson, J. B., Jampana, V., Weller, R. A., Bigorre, S. P., Plueddemann, A. J., Fairall, C. W., . . . Hersbach, H. (2013). On the exchange of momentum over the open ocean. *Journal of Physical Oceanography*, *43*(8), 1589–1610. doi: 10.1175/JPO-D-12-0173.1
- Fairall, C. W., Bradley, E. F., Hare, J. E., Grachev, A. A., & Edson, J. B. (2003). Bulk Parameterization of Air–Sea Fluxes: Updates and Verification for the COARE Algorithm. *Journal of Climate*.
- Fairall, C. W., Bradley, E. F., Rogers, D. P., Edson, J. B., & Young, G. S. (1996). Bulk parameterization of air-sea fluxes for Tropical Ocean-Global Atmosphere Coupled-Ocean Atmosphere Response Experiment. *Journal of Geophysical Research: Oceans*, *101*(C2), 3747–3764. doi: 10.1029/95JC03205
- Giglio, D., Gille, S. T., Subramanian, A. C., & Nguyen, S. (2017). The role of wind gusts in upper ocean diurnal variability. *Journal of Geophysical Research:*

- Oceans*, 122(9), 7751–7764. doi: 10.1002/2017JC012794
- Gleckler, P. J., & Weare, B. C. (1997). Uncertainties in Global Ocean Surface Heat Flux Climatologies Derived from Ship Observations. *Journal of Climate*, 10(11), 2764–2781. doi: 10.1175/1520-0442(1997)010<2764:UIGOSH>2.0.CO;2
- Guillaumin, A. P., & Zanna, L. (2021). Stochastic-Deep Learning Parameterization of Ocean Momentum Forcing. *Journal of Advances in Modeling Earth Systems*, 13(9). doi: 10.1029/2021MS002534
- Harrop, B. E., Ma, P.-L., Rasch, P. J., Neale, R. B., & Hannay, C. (2018). The Role of Convective Gustiness in Reducing Seasonal Precipitation Biases in the Tropical West Pacific. *Journal of Advances in Modeling Earth Systems*, 10(4), 961–970. doi: 10.1002/2017MS001157
- Hsu, C.-W., DeMott, C. A., Branson, M. D., Reeves Eyre, J., & Zeng, X. (2022). Ocean Surface Flux Algorithm Effects on Tropical Indo-Pacific Intraseasonal Precipitation. *Geophysical Research Letters*, 49(7), e2021GL096968. doi: 10.1029/2021GL096968
- Juricke, S., Palmer, T. N., & Zanna, L. (2017). Stochastic Subgrid-Scale Ocean Mixing: Impacts on Low-Frequency Variability. *Journal of Climate*, 30(13), 4997–5019. doi: 10.1175/JCLI-D-16-0539.1
- Large, W. G., McWilliams, J. C., & Doney, S. C. (1994). Oceanic vertical mixing: A review and a model with a nonlocal boundary layer parameterization. *Reviews of Geophysics*, 32(4), 363–403. doi: 10.1029/94RG01872
- Large, W. G., & Yeager, S. G. (2009). The global climatology of an interannually varying air–sea flux data set. *Climate Dynamics*, 33(2), 341–364. doi: 10.1007/s00382-008-0441-3
- Leufen, L. H., & Schädler, G. (2019). Calculating the turbulent fluxes in the atmospheric surface layer with neural networks. *Geoscientific Model Development*, 12(5), 2033–2047. doi: 10.5194/gmd-12-2033-2019
- Li, Q., Bruggeman, J., Burchard, H., Klingbeil, K., Umlauf, L., & Bolding, K. (2021). Integrating CVMix into GOTM (v6.0): a consistent framework for testing, comparing, and applying ocean mixing schemes. *Geoscientific Model Development*, 14(7), 4261–4282. doi: 10.5194/gmd-14-4261-2021
- McCandless, T., Gagne, D. J., Kosović, B., Haupt, S. E., Yang, B., Becker, C., & Schreck, J. (2022). Machine Learning for Improving Surface-Layer-Flux Estimates. *Boundary-Layer Meteorology*, 185(2), 199–228. doi: 10.1007/s10546-022-00727-4
- Nix, D., & Weigend, A. (1994). Estimating the mean and variance of the target probability distribution. In *Proceedings of 1994 IEEE International Conference on Neural Networks (ICNN'94)* (Vol. 1, pp. 55–60 vol.1). doi: 10.1109/ICNN.1994.374138
- Nuijens, L., Wenegrat, J., Lopez Dekker, P., Pasquero, C., O'Neill, L. W., Arduin, F., ... Laurindo, L. C. (2024). The Air-Sea Interaction (ASI) submesoscale: physics and impact. In *Lorentz Workshop*.
- Polichtchouk, I., & Shepherd, T. G. (2016). Zonal-mean circulation response to reduced air–sea momentum roughness. *Quarterly Journal of the Royal Meteorological Society*, 142(700), 2611–2622. doi: 10.1002/qj.2850
- Popinet, S. (2020). A vertically-Lagrangian, non-hydrostatic, multilayer model for multiscale free-surface flows. *Journal of Computational Physics*, 418, 109609.
- Schreck, J. S., Gagne, D. J., Becker, C., Chapman, W. E., Elmore, K., Fan, D., ... Wirz, C. (2024). Evidential Deep Learning: Enhancing Predictive Uncertainty Estimation for Earth System Science Applications. *Artificial Intelligence for the Earth Systems*. doi: 10.1175/AIES-D-23-0093.1
- Umlauf, L., & Burchard, H. (2005). Second-order turbulence closure models for geophysical boundary layers. A review of recent work. *Continental Shelf Research*, 25(7), 795–827. doi: 10.1016/j.csr.2004.08.004
- Williams, P. D. (2012). Climatic impacts of stochastic fluctuations in air–sea

- fluxes. *Geophysical Research Letters*, *39*(10), 2012GL051813. doi: 10.1029/2012GL051813
- Yu, L. (2019). Global Air–Sea Fluxes of Heat, Fresh Water, and Momentum: Energy Budget Closure and Unanswered Questions. *Annual Review of Marine Science*, *11* (Volume 11, 2019), 227–248. doi: 10.1146/annurev-marine-010816-060704
- Zhou, S., Shi, R., Yu, H., Zhang, X., Dai, J., Huang, X., & Xu, F. (2024). A Physical-Informed Neural Network for Improving Air-Sea Turbulent Heat Flux Parameterization. *Journal of Geophysical Research: Atmospheres*, *129*(17), e2023JD040603. doi: 10.1029/2023JD040603